Desalination and Water Treatment
www.deswater.com

doi: 10.5004/dwt.2017.20615

75 (2017) 225–236
May

Efficient biosorption of methylene blue, malachite green and methyl violet organic pollutants on biomass derived from *Anethum graveolens*: an eco-benign approach for wastewater treatment

A. Hamitouche, M. Haffas, A. Boudjemaa, S. Benammar, M. Sehailia*, K. Bachari

Centre de Recherche Scientifique et Technique en Analyses Physico-chimiques (CRAPC), BP 384-Bou-Ismail-RP 42004, Tipaza, Algeria, emails: moussa.sehailia@crapc.dz (M. Sehailia), ahamitouche2@yahoo.fr (A. Hamitouche), youba54@yahoo.com (M. Haffas), amel_boudjemaa@yahoo.fr (A. Boudjemaa), souad.benammar@yahoo.fr (S. Benammar), bachari2000@yahoo.fr (K. Bachari)

Received 24 July 2016; Accepted 21 February 2017

ABSTRACT

Three organic pollutants belonging to the class of cationic dye, namely methylene blue (MB), malachite green (MG) and methyl violet (MV), were successfully removed from aqueous solutions using biomass derived from *Anethum graveolens* (*A. graveolens*). Factors such as pH (3–10), stirring speed (100–400 rpm), biosorbent concentrations (0.5–3 g L^{-1}) and initial dyes' concentrations (10–50 mg L^{-1}) were all studied to attain the maximum removal efficiency for all three dyes. Prior to the biosorption process, the morphology of the biomaterial was characterized using scanning electron microscopy. Fourier transform infrared spectroscopy analysis of the biosorbent demonstrated the presence of key functional groups associated with the biosorption phenomenon such as those of amino, carboxyl, hydroxyl and carbonyl groups. The obtained results showed that the optimal conditions are 300 rpm for stirring speed, 4, 6 and 7 for pH, 3 g L^{-1} for biomass dosage and 10 mg L^{-1} for dyes' concentrations. Removal efficiency augmented from 56% to 99% for all pollutants. The kinetic sorption was described by the pseudo-second-order kinetic equation (R^2 = 0.997). The isotherm sorption was described by the Sips and Freundlich models for MV removal (R^2 = 0.998 and 0.991, respectively). The Langmuir (R^2 = 0.991), Sips (R^2 = 0.997) and Temkin (R^2 = 0.997) models were best fitted for MG removal; however, for MB removal, it was found that Freundlich (R^2 = 0.993), Sips (R^2 = 0.997) and Langmuir (R^2 = 0.999) models were best to explain the sorption phenomenon. At optimum conditions, the maximum biosorption capacity (q_{max}) was ca. 833, 833 and 244 mg g^{-1} for MB, MV and MG, respectively.

Keywords: Anethum graveolens; Biosorption; Cationic dyes; Isotherm models; Kinetic models

1. Introduction

Dyes are complex chemical structures stabilized by their aromatic character. The discharge of industrial effluents containing dyes in wastewater can create potential risks and toxicity problems for the wider community; most dyes are difficult to remove during wastewater treatment [1]; they also tend to exhibit high stability and resistance to chemical degradation. In order to limit the amount of dyes disposed to the environment, many countries imposed stringent regulations that would ensure that dyes are used responsibly by the wider industrial community; in this respect, such approach encouraged researchers to explore cost-effective methods that are capable to remove dyes from large volumes of effluents [2].

Many methods are used to remove dyes from wastewater; this includes coagulation/flocculation, sedimentation, adsorption, membrane separation, ozonation, electrochemical techniques and advanced oxidation [3–9].

One of the cheapest and facile wastewater treatment strategies currently used is adsorption on activated carbon. Unfortunately, over the past few years, many researchers

* Corresponding author.

found that this process has limited applications and can be expensive compared with other much cheaper biosorption techniques [10,11].

For this reason, developing simple and cheap alternative processes such as those based on biosorption had attracted a considerable attention from the wider scientific community [12,13]. To maximize the efficiency of the overall process, the following factors must be taken into account: (i) the necessity to utilize a minimum amount of biosorbent material during the purification of water, (ii) facile regeneration of the biosorbent substance following purification [14–19], (iii) renewability of the source, (iv) low cost and (v) the high sorption capacity of the material used [4].

The necessity to adhere to the aforementioned factors prompted scientists to continue searching for other readily available biosorbent materials that would respond to the current needs in wastewater treatment [10,11].

It has been acknowledged in literature that a number of biosorbents including bacteria [20], fungi [21], yeast [22], algae [23] and other agricultural waste [24] have indomitable affinity to bind to pollutants.

Recently, numerous research studies have been published with the aim of finding more cheaper and much effective biosorbents derived from agricultural wastes, e.g., wood sawdust, rice husk, sugarcane bagasse, orange peels and coffee beans [25–29]. The agricultural by-products could be assumed to be low-cost biosorbents, since they are abundant in nature and require little processing [30]. Different biosorbents formulated in powder form have been tested for their ability to remove dyes from wastewater [31–33].

In searching for a better biosorbent, our group has elected to exploit the utilization of biomass derived from *Anethum graveolens* (*A. graveolens*) to affect the biosorption of three major dyes found in the effluents of many industrial sites working in the field of pigments. The aim of the present work is to study the removal efficiency of methylene blue (MB), malachite green (MG) and methyl violet (MV) using materials derived from biomass. *A. graveolens* is the sole species of the genus *Anethum*, classified by some botanists in the related genus *Peucedanum* as *Peucedanum graveolens* (L.) [34]. Various experimental factors such as pH, amount of biosorbent, agitation and the initial dye concentration were investigated.

2. Materials and methods

2.1. Biosorbent preparation and characterization

The plant was collected from the north of Algeria in the municipality of Kolea, located 28 km from southwest of Algiers. The material was washed several times with bidistilled water and dried in oven at 60°C followed by crushing and sieving in order to obtain a diameter between 200 and 400 μm; the final product was stocked for use in biosorption experiments. The surface morphology of the biosorbent has been characterized by scanning electron microscopy with energy dispersive X-ray analysis (SEM–EDX) using FEI Quanta 250. The images show the characteristics of the surface texture of the biomass prior to the biosorption process of dye. The biomass' functional groups present prior to and after the tests were determined by Fourier transform infrared (FTIR) spectroscopy. FTIR spectra were obtained using Bruker Alpha-p spectrometer over the range 4,000–400 cm^{-1}.

2.2. Adsorbate

MB, MG and MV were supplied by Aldrich Chemical Co. (USA). Stock solutions of dyes were prepared by dissolving a weighed amount of the dye in 1 L of bidistilled water to obtain a concentration of 1,000 mg L^{-1}. Samples of various concentrations were prepared by further dilution of stock solutions.

2.3. Biosorption experiments

The biosorption tests were carried out in a batch reactor (IKA, Bou-Ismail, KS 130) at room temperature (25°C). The biomass was dispersed in 50 mL of dye solutions (MB, MG and MV). The experiments were performed at different pH values controlled by the addition of HCI or NaOH solutions. The residual concentrations were determined using UV spectrophotometer (SPECORD 210 plus, Analytik-Jena, Bou-Ismail). The maximum absorption wavelengths were 663, 622 and 588 nm for MB, MG and MV, respectively. All batch sorption experiments were carried out in duplicates under identical conditions. Before analysis, the liquid samples were centrifuged (3,000 rpm) for 20 min. The removal efficiency Y (%), the equilibrium (q_e) and the sorption capacity (q_t) were determined using the following equations [35]:

$$Y(\%) = \frac{C_0 - C_e}{C_0} \times 100 \tag{1}$$

$$q_t = \frac{C_0 - C_t}{m} \times V \tag{2}$$

$$q_e = \frac{C_0 - C_e}{m} \times V \tag{3}$$

The kinetic parameters are calculated using non-linear pseudo-first-order (Eq. (4)), pseudo-second-order (Eq. (5)), and Elovich (Eq. (6)) models, Bangham's equation (Eq. (7)) and intraparticle diffusion (Eq. (8)) model [36,37]:

$$q_t = q_e\left(1 - e^{-k_1 t}\right) \tag{4}$$

$$q_t = \frac{k_2 q_e^2 t}{1 + k_2 q_e t} \tag{5}$$

$$q_t = \frac{1}{\beta}\ln(\alpha\beta) + \frac{1}{\beta}\ln t \tag{6}$$

$$\log\left(\frac{C_0}{C_0 - m\,q_t}\right) = \log\left(\frac{m\,k_{0B}}{2.303\,V}\right) + \alpha_B \log(t) \tag{7}$$

$$q_t = k_{\text{diff}}\, t^{0.5} + C \tag{8}$$

The sorption isotherms were performed using a range of biomass concentrations. The data were analyzed using Freundlich

(Eq. (9)), Langmuir (Eq. (10)), Dubinin–Radushkevich (Eq. (11)), Temkin (Eq. (16)), Sips (Eq. (17)), Toth (Eq. (18)), Khan (Eq. (19)) and Redlich–Peterson (R–P; Eq. (20)) isotherm models [38]:

$$\ln q_e = \ln K_F + \frac{1}{n}\ln C_e \tag{9}$$

$$\frac{1}{q_e} = \frac{1}{q_m} + \frac{1}{K_L\, q_m}\frac{1}{C_e} \tag{10}$$

$$\ln q_e = \ln q_m - k_{D-R}\,\varepsilon^2 \tag{11}$$

$$q_e = \frac{RT}{b}\ln\left(K_T C_e\right) \tag{12}$$

The constant $k_{D–R}$ gave the mean free energy (E) of sorption per sorbate molecule when it was transferred to the biomass surface from infinity in the solution and can be computed using the following relationship [39]:

$$E = \frac{1}{\sqrt{2k_{D-R}}} \tag{13}$$

$$B_1 = \frac{RT}{b} \tag{14}$$

Furthermore, the dimensionless separation factor (R_L; Eq. (12)) was determined using the Langmuir constant (K_L; L mg^{-1}) to ascertain the favorability of the sorption [40].

$$\mathrm{R_L} = \frac{1}{1+\mathrm{K_L C_0}} \tag{15}$$

$$q_e = \frac{RT}{b}\ln K_T + \frac{RT}{b}\ln C_e \tag{16}$$

$$q_e = \frac{q_m\, a_S\, C_e^{1/n}}{1+a_S\, C_e^{1/n}} \tag{17}$$

$$q_e = \frac{q_{mT}\; C_e}{\left(1/K_T + C_e^{m_T}\right)^{1/m_T}} \tag{18}$$

$$q_e = \frac{q_m\, b_K\, C_e}{\left(1+a_S\, C_e\right)^{a_K}} \tag{19}$$

$$q_e = \frac{K_{R-P}\, C_e}{1+a_{R-P}\, C_e^{\beta}} \tag{20}$$

All data were analyzed using MATLAB7.0, STATISTICA7.0 and EXCEL to obtain kinetic and isotherm parameters.

3. Results and discussion

3.1. Biosorbent characterization before and after biosorption

3.1.1. Morphology analysis

The surface morphology of the biomass was examined using SEM–EDX. In order to rule out any negative aspects, the biomass was pre-dried in a forced-air oven at 60°C for 4 d before being analyzed. The biomass was mounted on SEM, and the surface of the sample was then scanned at the desired magnifications (1,600×, 3,000× and 10,000×). It was observed that the biomass possesses a hierarchical and irregular shapes (Fig. 1(a)) with unstructured pores present in low numbers (Figs. 1(b) and (c)).

Microscopy observations (Fig. 1) showed that the surface of the biomass is fairly rough, providing a large exposed surface area for better adsorption of dyes. The porous nature of the biomass structure reduces diffusion resistance and thus facilitates the mass transfer of dyes.

3.1.2. EDX analysis

The effective atomic concentration of the different constituents present on top of the surface layers of the specimen was investigated using EDX at three different areas with voltage of 10.0 keV.

Fig. 1(c) shows the obtained biomass primarily consisting of carbon and oxygen. All elements are clearly observed at their corresponding keV values. The quantitative analyses of the EDX spectra are given in Fig. 1(d) and Table 1.

The observation from the table may report that the surface concentration of carbon and oxygen species at 10 keV on three different areas over the surface of specimen is much closer to each other. This finding shows the homogeneity of the composition of biomass.

3.1.3. FTIR–ATR analysis

A. graveolens is composed of numerous functional groups as confirmed by the presence of various absorption peaks in the FTIR spectra. The spectra obtained before and after the sorption of cationic dyes are almost identical and regrouped in Fig. 2. The results were significantly similar, suggesting that the *A. graveolens* structure remained intact after biosorption tests. FTIR spectrum of fresh *A. graveolens* (Fig. 2(b)) showed bands located at 3,340 cm^{-1} (O–H/N–H), 2,919 cm^{-1} (C–H), 2,854 cm^{-1} (C–H), 1,726 cm^{-1} (C=O), 1,600 cm^{-1} (C=C), 1,158 cm^{-1} (C–O), 1,025 cm^{-1} (C–O) and 896 cm^{-1} (bending aromatic C–H) [41]. In parallel, some bands increased or decreased sharply after biosorption; this was primarily due to the dyes' interaction with different functional groups. We also note great similarities between the fresh biomass' FTIR spectra and that after MG biosorption; this was not the case with MB and MV dyes spectra. FTIR spectra also showed shifting of some infrared absorption peaks to new values (Figs. 2(c) and (a)), confirming the interaction between the corresponding functional groups and both dyes during the biosorption process [42].

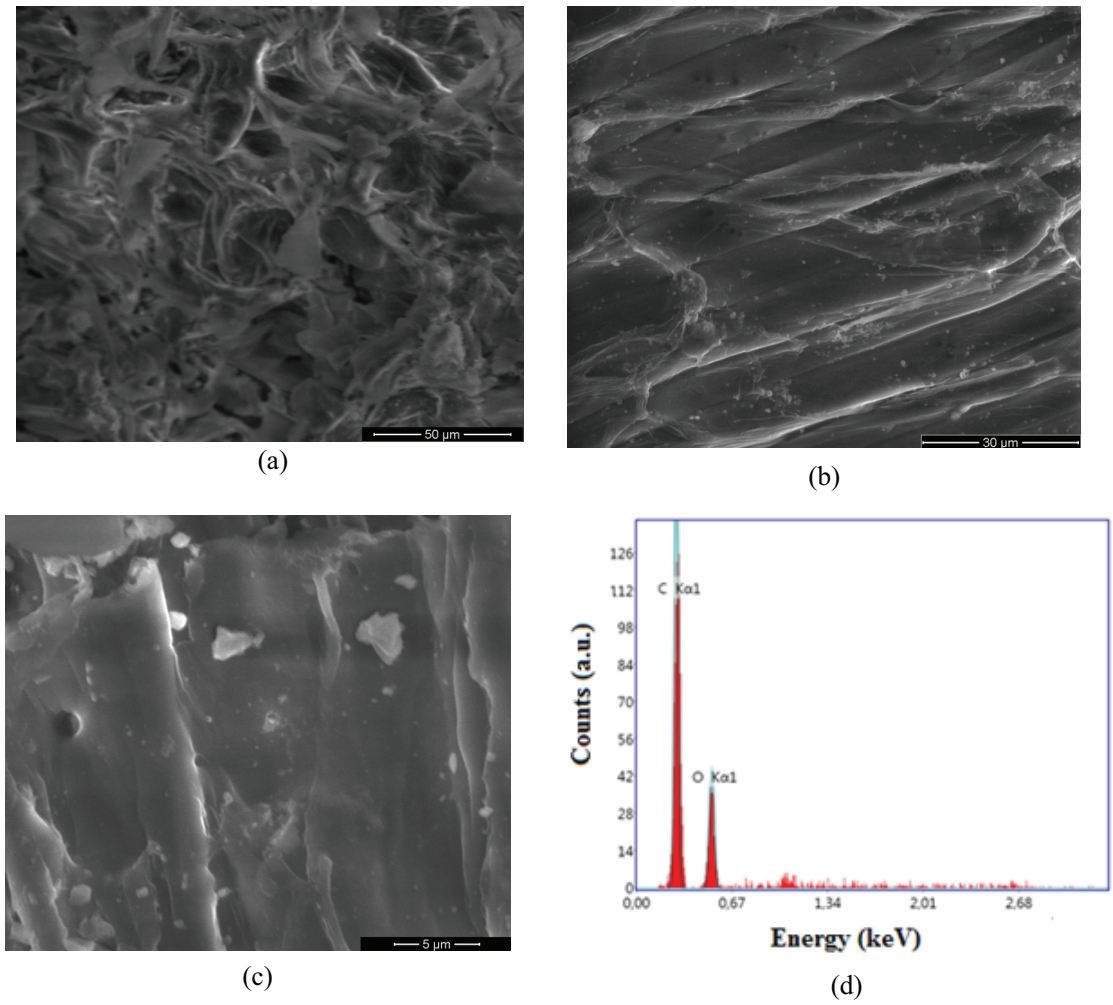

Fig. 1. (a)–(c) Scanning electron microscopy (SEM) image of the biomass with various magnifications and (d) EDS spectrum of *A. graveolens*.

Table 1
EDX line spectra

Element (k)	Area 1		Area 2		Area 3	
	Wt%	Atomic %	Wt%	Atomic %	Wt%	Atomic %
C	65.51	71.68	67.06	73.06	66.23	72.32
O	34.49	28.32	32.94	26.94	33.77	27.68

3.2. Optimization of process parameters

Experimental studies were performed to study the effects of different parameters, i.e., stirring speed (100–400 rpm), pH (3–10), biosorbent dose (0.5–3 g L^{-1}), initial dyes' concentration (10–50 mg L^{-1}) and contact time on the dyes removal efficiency.

3.2.1. Effect of stirring speed

The stirring speed is an important parameter that influenced the biomass distribution. This effect was studied at

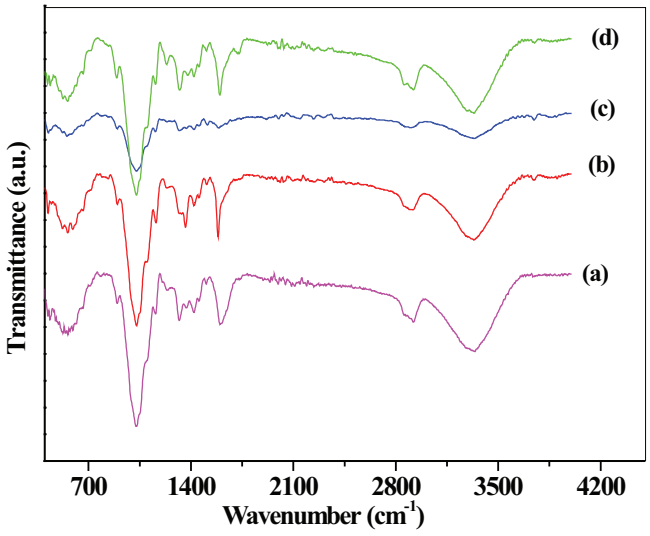

Fig. 2. FTIR spectra of a fresh biomass (b) and after biosorption using: (c) MB, (d) MG and (a) MV.

room temperature for biosorbent dose of 1 g L^{-1} and pH 9.14, 5.78 and 7.12 for MB, MG and MV, respectively. The results regrouped in Fig. 3 showed that the removal efficiency

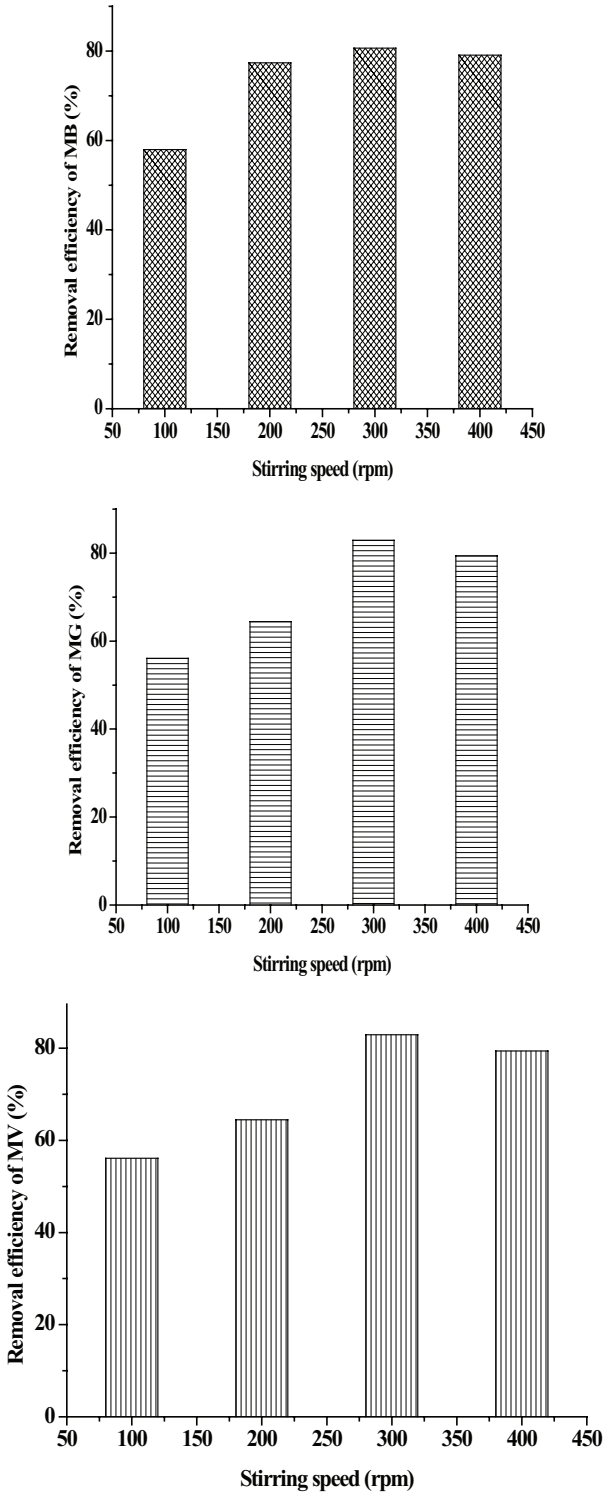

Fig. 3. Effect of stirring speed value on the efficiency sorption removal of dyes after 180 min of reaction: C_0 = 50 mg L^{-1}, *A. graveolens* dose = 1 g L^{-1} and pH = 9.14, 5.78 and 7.12 for MB, MG and MV, respectively.

increased to reach maxima at 300 rpm with a removal efficiency of 80.6%, 82.9% and 80.8% for MB, MG and MV, respectively, then decreased to 400 rpm [43,44]. In the present study, this phenomenon seemed to be affected by a high stirring speed. So, the turbulence caused by agitation enhanced the dyes' mass transfer from the bulk solution to the biomass surface. This transfer helped the dyes to be fixed on the biomass surface and improved the sorption process. Thus, the decrease in removal efficiency may be attributed to the formation of boundary layer thickness around the biomass, leading to a decrease in adequate mixing and equally the vortex phenomena, which can reduce the external diffusion of dyes in the sorption processes.

3.2.2. Effect of initial pH

The effect of initial pH on the sorption process is one of the significant factors governing the uptake process since it can directly influence the solute's dissociation, biomass surface charge and heterogeneity. The pH effect was studied at room temperature, biosorbent dose 1 g L^{-1} and contact time 4 h (Fig. 4). The dyes removal efficiency augmented with increasing pH until maxima (82.6%, 83% and 80.8% for MB, MG and MV, respectively); above the optimal pH values, the removal efficiency decreased. The optimal pH was 4.02, 5.78 and 7.12 for MB, MG and MV, respectively [45,46], indicating that the biosorption is strongly dependent on pH value, which is also explained by the point zero charge (pH_{pzc}).

pH_{pzc} plays an important role to explain the sorption mechanism [47]. In our case, the pH_{pzc} (3.72) of *A. graveolens* was measured using the solid addition method (Fig. 5) [48]. This result indicated that the dyes biosorption is dependent on both pH value and the charge repartition on biomass surface [46,49]. At low pH, the biosorption capacity was lower due to the presence of large amount of protons that can compete with dye ions binding at the sorption site (Fig. 4). When the pH was increased, the negatively charged sorption sites facilitate the dye ions biosorption. Therefore, at high pH values, precipitation inhibits the contact between the dye and the biosorbent [50].

3.2.3. Effect of A. graveolens dosage

The results showing the effect of biomass dosage are regrouped in Fig. 6. The graphs indicated that when the biomass dosage was increased from 0.5 to 3 g L^{-1}, the removal efficiency increased from 68.27% to 93.52%, 65.98% to 93.21% and 68.61% to 93.71% for MB, MG and MV, respectively. On the other hand, the sorption capacity of biomass decreased from 77.25 to 18.88 mg g^{-1}, 58.54 to 15.18 mg g^{-1} and 72.87 to 16.87 mg g^{-1}, for MB, MG and MV, respectively. Our results are similar to other works, which showed that increasing the sorbent dose resulted in the reduction of sorption capacity [36,51–54].

At higher biosorbent doses, the competition of sorbate for the available active sites permitted a steady uptake of all dyes above the optimal concentration. Such phenomenon is attributed to the limited number of active sites, less availability of solute, a minimum or low level of electrostatic interaction, and an intrusion between the binding sites [3–6]. In addition, the surface of the biosorbent gets saturated at

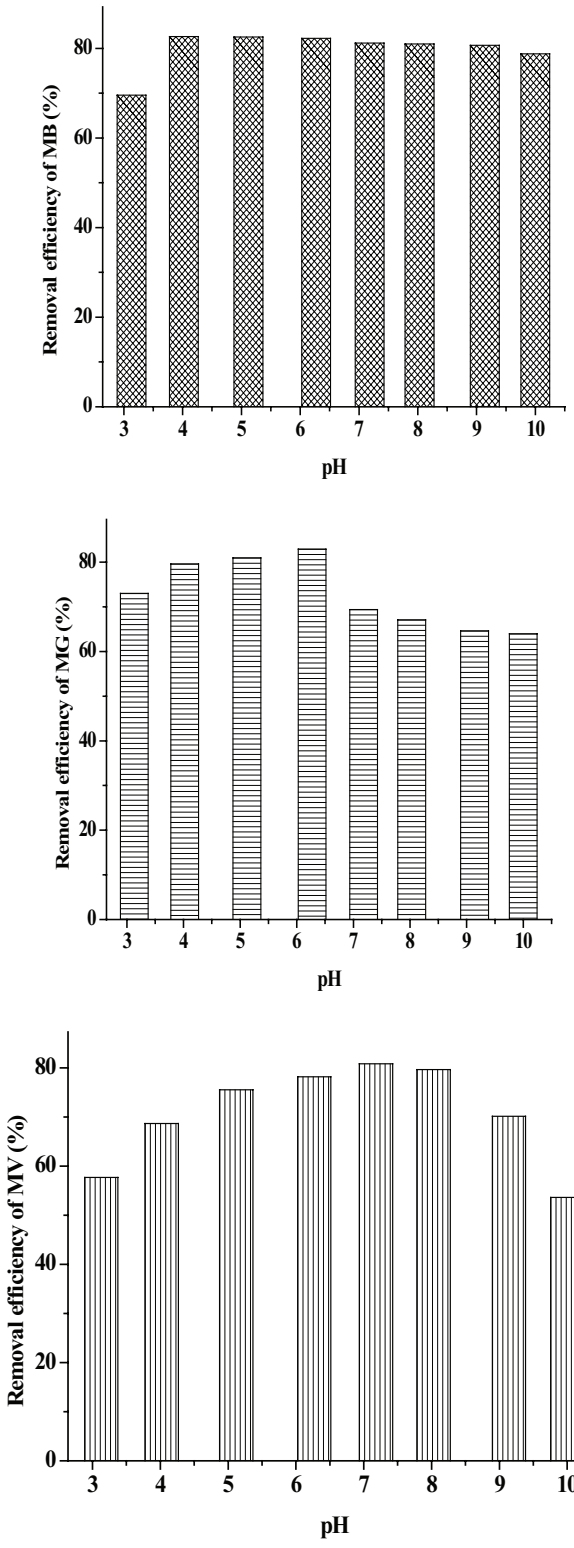

Fig. 4. Effect of pH value on the efficiency sorption removal of dyes after 180 min of reaction: C_0 = 50 mg L^{-1}, *A. graveolens* dose = 1 g L^{-1} and stirring rate of 300 rpm.

higher concentrations due to the screening effect [6,55,56], thus protecting the binding of adsorbates, which resulted in the less biosorption capacity.

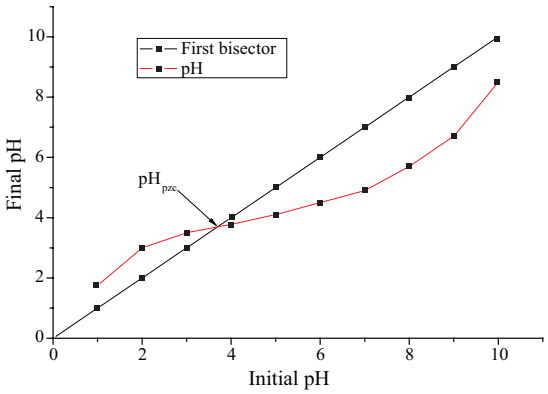

Fig. 5. Evolution of final pH vs. initial pH.

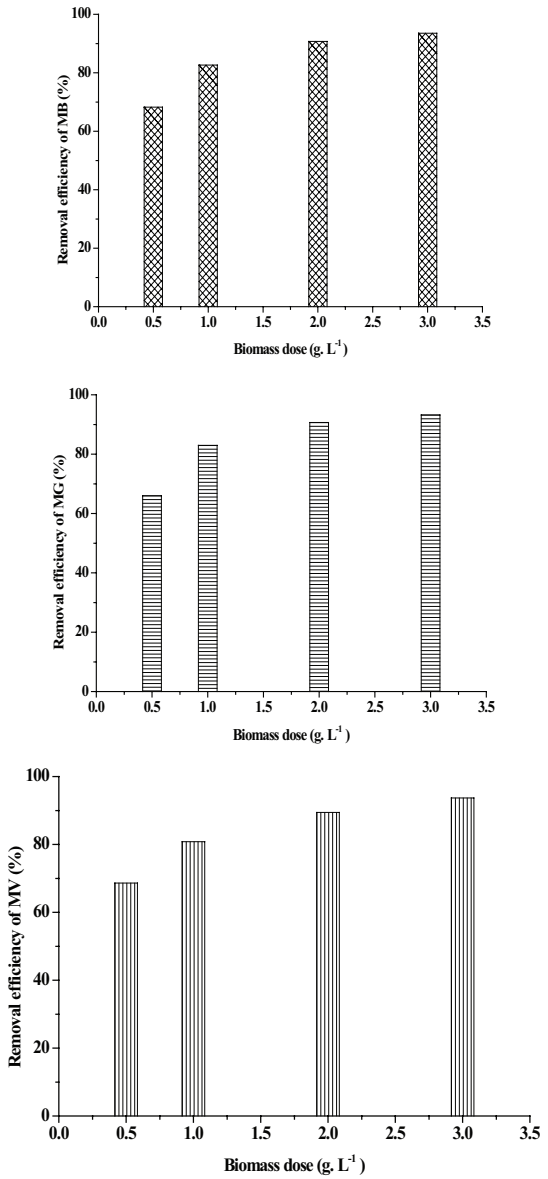

Fig. 6. Effect of biomass dose on the efficiency removal of dyes after 180 min of reaction at optimal pH, stirring speed = 300 rpm and C_0 = 50 mg L^{-1}.

3.3. Kinetic studies

3.3.1. Sorption kinetic

In order to determine the relationship between dyes' concentration and sorption efficiency, our study focused on the variation of the initial concentration (10–50 mg L^{-1}) vs. time. It is obvious that the amount of biosorbed material increased with the initial dye's concentration (Figs. 7–9). So, biosorption capacity strongly depended on the initial concentration. The sorption capacity at equilibrium q_e increased from 10.68 to 49.26 mg g^{-1}, 9.99 to 41.94 mg g^{-1} and 10.71 to 43.52 mg g^{-1}, while the initial concentration of dyes (MB, MG and MV, respectively) augmented from 10 to 50 mg L^{-1}. As shown in Figs. 7–9, the sorption was rapidly increased in the first 30 min, which involved the physical sorption of dyes at the biosorbent surface. After the initial step, the sorption capacity was moderate due to both saturation of binding sites and slow intracellular diffusion. Many studies reported similar results related to the behavior of organic compounds' biosorption on biomass. The equilibrium was attained to nearly 180 min while the maximum dye sorption capacity augmented from 82.66% to 98.94%, 82.98% to 98.98% and 80.81% to 97.93% for MB, MG and MV, respectively. It is important to study the reaction rate at which the dye's concentration was reduced.

When dyes' concentrations increased from 10 to 50 mg L^{-1}, the amount of sorbed dyes increased from 10.68 to 49.26 mg g^{-1}, from 9.99 to 41.94 mg g^{-1} and from 10.71 to 43.52 mg g^{-1} for MB, MG and MV, respectively.

These results show that the initial dye's concentration plays an important role in affecting the capacity of dyes to sorb onto vegetal biomass.

Many authors described that high dyes' concentrations lead to a higher concentration gradient and therefore higher sorption capacity [3–11].

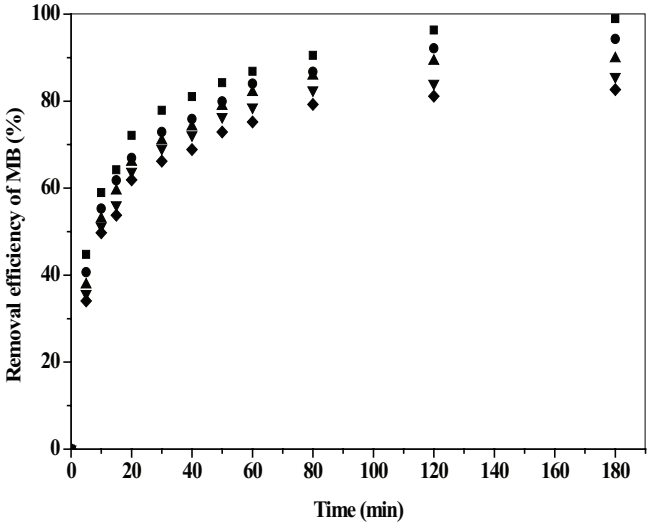

Fig. 7. Effect of initial concentration of dyes on the efficiency biosorption removal of MB vs. time under reaction conditions: stirring speed = 300 rpm, *A. graveolens* dose = 1 g L^{-1} and pH = 4.02: (■) 10, (●) 20, (▲) 30, (▼) 40 and (♦) 50 mg L^{-1}.

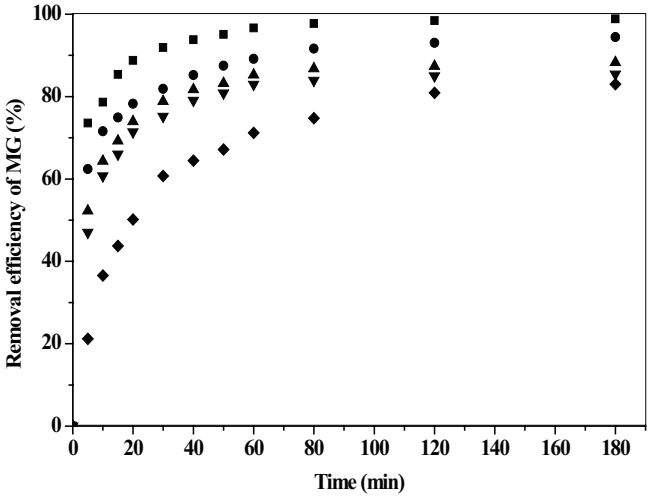

Fig. 8. Effect of initial concentration of dyes on the efficiency biosorption removal of MG vs. time under reaction conditions: stirring speed = 300 rpm, *A. graveolens* dose = 1 g L^{-1} and pH = 5.78: (■) 10, (●) 20, (▲) 30, (▼) 40 and (♦) 50 mg L^{-1}.

3.3.2. Kinetic models

To investigate the treatment process of dyes on *A. graveolens*, five kinetic models have been studied namely pseudo-first-order, Elovich, pseudo-second-order, Bangham's and intraparticle diffusion models. These models were most commonly used to describe the kinetic models for the dyes' sorption [57–59]. The results were regrouped in Table 2(a), which shows that when dyes' concentrations increased from 10 to 50 mg L^{-1}, the correlation coefficient (R^2) values augmented from 0.9504 to 0.9802, 0.909 to 0.9822 and 0.8931 to 0.9897 for pseudo-first-order kinetic model for MB, MG and MV, respectively. On the other hand, for Elovich model, R^2 increased in range from 0.9557 to 0.9843, 0.9102 to 0.9799 and 0.7715 to 0.9662 for MB, MG and MV, respectively.

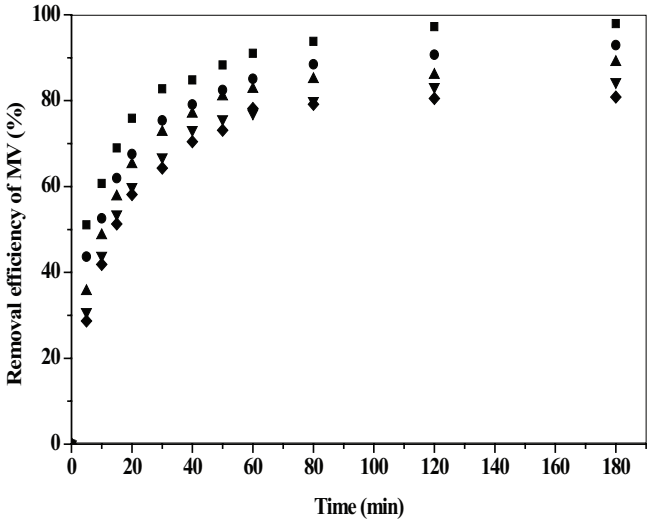

Fig. 9. Effect of initial concentration of dyes on the efficiency biosorption removal of MV vs. time under reaction conditions: stirring speed = 300 rpm, *A. graveolens* dose = 1 g L^{-1} and pH = 7.12: (■) 10, (●) 20, (▲) 30, (▼) 40 and (♦) 50 mg L^{-1}.

Table 2(a)
Constant of kinetic models

	Conc. (mg L^{-1})	$q_{e\text{-exp}}$ (mg g^{-1})	Pseudo-first-order model			Elovich equation			Pseudo-second-order model		
			$k_1 \times 10^2$ (min^{-1})	$q_{e\text{-mod}}$ (mg g^{-1})	R^2	α (mg g^{-1} min^{-1})	B (g mg^{-1})	R^2	$k_2 \times 10^3$ (g mg^{-1} min^{-1})	$q_{e\text{-mod}}$ (mg g^{-1})	R^2
BM	10	10.68	2.314	2.211	0.9504	7.872	0.609	0.9841	9.677	11.136	0.999
	20	19.77	2.436	2.957	0.9634	12.055	0.317	0.9843	4.974	20.704	0.9991
	30	26.98	3.329	3.619	0.9802	15.665	0.224	0.9682	4.497	26.667	0.9997
	40	34.82	2.822	3.735	0.9604	21.195	0.174	0.9557	3.296	36.496	0.9998
	50	49.26	2.761	4.363	0.964	29.492	0.123	0.9579	2.259	51.546	0.9972
MG	10	9.99	3.492	1.644	0.9119	7713.127	1.323	0.9215	39.488	10.141	0.9999
	20	19.26	2.700	2.408	0.909	447.236	0.535	0.9735	11.625	19.685	0.9998
	30	26.58	3.147	2.819	0.9099	183.403	0.328	0.921	8.896	27.247	0.9999
	40	34.99	3.634	3.401	0.9594	130.157	0.228	0.9102	6.278	35.971	0.9999
	50	41.94	2.497	4.539	0.9822	7.270	0.111	0.9799	1.379	45.662	0.9997
MV	10	10.712	3.208	2.232	0.9722	14.777	0.656	0.9615	13.272	11.123	0.9997
	20	18.78	2.578	2.790	0.9483	13.502	0.336	0.9662	6.193	19.607	0.9998
	30	26.78	2.497	3.198	0.8931	13.109	0.215	0.9396	4.248	28.011	0.9998
	40	33.04	2.944	3.809	0.9744	12.183	0.163	0.949	2.981	34.965	0.9999
	50	43.53	4.081	4.662	0.9897	0.119	1.065	0.7715	2.354	46.296	0.9991

These results have shown that the experimental data were not established according to both pseudo-first-order kinetic model and Elovich model.

Table 2(a) shows clearly that the experimental data were established according to a pseudo-second-order kinetic model for the three dyes. The correlation coefficients exceeded 0.999. However, the second-order rate constant (k_2) decreased with increasing the initial dyes concentration. Similar observations were reported for the removal of organic and inorganic compounds from aqueous solutions [3–12,36,60]. As the vacant sites on *A. graveolens* became occupied, higher initial concentrations resulted in a reduction in removal efficiency since the available number of dye molecules in solution exceeded the biosorption capacity of *A. graveolens* [40,61].

The intraparticle diffusion is usually involved in the sorption process; the plot of the square root of time vs. the uptake (q_t) would result in a linear relationship.

The k_{diff} values were calculated by using correlation analysis (Table 2(b)); the value of this parameter grows with increasing the initial dyes' concentration.

The correlation coefficients varied from 0.928 to 0.987. These values are close to unity, thus indicating the application of this model. The functional relationship corresponds to the characteristic of intraparticle diffusion. The intraparticle diffusion plots have been given in Fig. 10.

The intraparticle diffusion could be the controlling step if the line is passed through origin. The values of intercept in Fig. 10 can provide us with an idea about the boundary layer thickness. In our case, the plots do not pass through origin, which signified that the process was partially controlled by the boundary layer; this had also indicated that the intraparticle diffusion is not the only rate-controlling step but other processes may also control the rate of sorption, i.e., the larger the intercept, the bigger the boundary layer effect [62]. Similar results were obtained for basic red 22 on pith [63], MB on perlite [64] and on montmorillonite [8], and MV on clinoptilolite [12].

Table 2(b)
Constant of intraparticle diffusion model and Bangham's equation

		Intraparticle diffusion model		Bangham's equation		
	Con. (mg L^{-1})	k_{diff}	R^2	α	k_{0B} (g)	R^2
MB	10	1.284	0.984	0.787	52.635	0.999
	20	2.487	0.961	0.607	67.423	0.991
	30	3.858	0.928	0.452	86.469	0.971
	40	4.664	0.979	0.456	83.437	0.953
	50	7.118	0.966	0.394	90.169	0.954
MG	10	0.709	0.987	0.367	138.848	0.988
	20	1.425	0.968	0.312	128.751	0.994
	30	2.882	0.976	0.302	120.528	0.943
	40	4.399	0.974	0.311	114.124	0.924
	50	5.325	0.971	0.549	64.928	0.962
MV	10	1.417	0.986	0.611	77.687	0.991
	20	2.530	0.970	0.579	73.192	0.957
	30	3.491	0.984	0.4572	87.364	0.951
	40	4.409	0.976	0.4587	81.809	0.947
	50	4.648	0.965	0.3559	96.456	0.937

Kinetic data were further used to know about the slow step occurring in the present sorption system using Bangham's equation [8].

The double logarithmic plot did not yield satisfactory linear curves for the removal of dyes onto *A. graveolens* ($0.924 \leq R^2 \leq 0.999$). This showed that the film diffusion was not the only rate-controlling parameter. It may be concluded that the film and pores diffusion were important to different extents in the removal process [8].

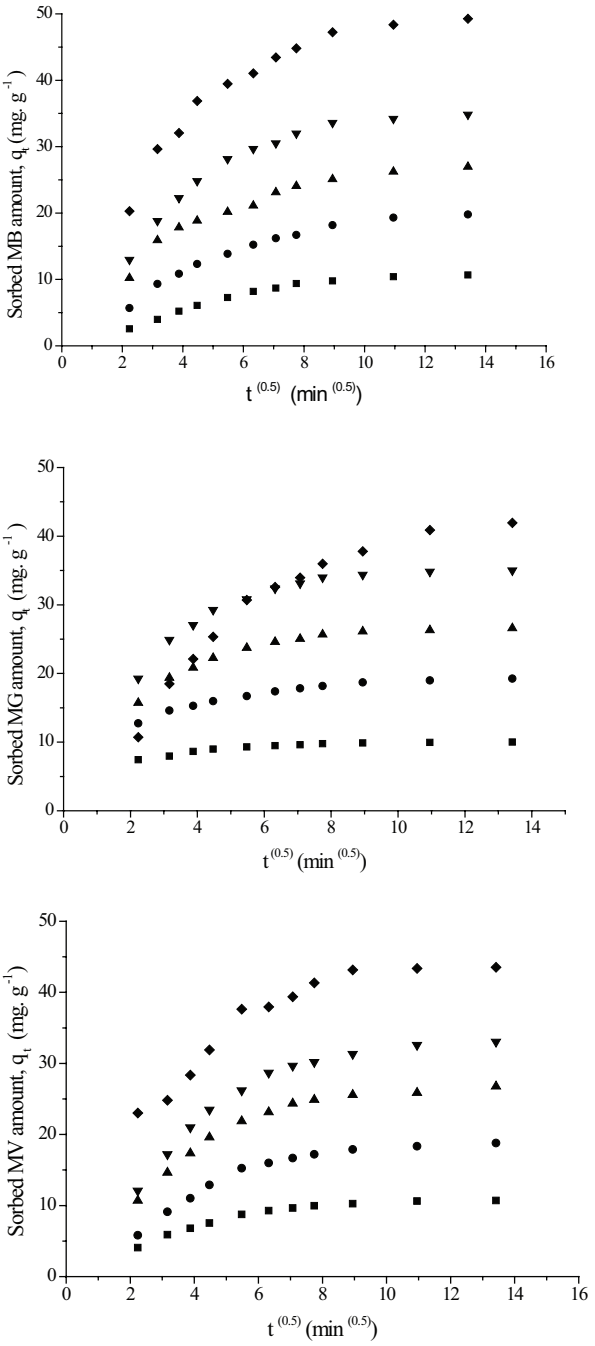

Fig. 10. Effect intraparticle diffusion plots for biosorption of dyes on *A. graveolens* at different initial dye concentrations: stirring speed = 300 rpm, *A. graveolens* dose = 1 g L^{-1} at optimal pH: (■) 10, (●) 20, (▲) 30, (▼) 40 and (♦) 50 mg L^{-1}.

3.4. Isotherm models

To optimize the design of a sorption system, it is important to establish the most appropriate correlation for the equilibrium curves. Several isotherm equations are found by many authors to describe the equilibrium isotherm. In this study, Freundlich, Langmuir, Dubinin–Radushkevich, Temkin, Sips, Toth, R–P and Khan models are used to describe this phenomenon (Table 3).

Table 3
Constants of Langmuir, Langmuir, Dubinin–Radushkevich, Temkin, Sips, Toth, Khan and Redlich–Peterson isotherms models

Isotherms models	Models constants	MB	MG	MV
Langmuir	q_m (mg g^{-1})	833.333	833.333	243.902
	K_L (L mg^{-1})	0.006	0.006	0.021
	R_L	0.770	0.777	0.485
	R^2	0.999	0.991	0.984
Freundlich	K_F (L mg^{-1})	5.466	5.537	5.156
	n	1.079	1.117	1.079
	R^2	0.997	0.982	0.991
Dubinin–Radushkevich	q_m (mg g^{-1})	67.952	56.328	57.208
	K_{D-R} (mol kJ^{-1})^2	4.348	3.262	3.287
	E (kJ mol^{-1})	0.339	0.391	0.389
	R^2	0.906	0.956	0.811
Temkin	B_1 (J mol^{-1})	38.482	29.09	34.675
	B	64.429	85.231	71.503
	K_t (L g^{-1})	0.382	0.491	0.409
	R^2	0.978	0.997	0.925
Sips	Q_s (mg g^{-1})	310.212	131.774	138.074
	K_s (L g^{-1})^{ns}	0.015	0.030	0.0344
	N_s	0.926	0.813	0.900
	R^2	0.993	0.994	0.998
Toth	Q_T (mg g^{-1})	362.533	82.168	278.420
	B_T	0.013	0.056	0.016
	n_T	0.100	0.357	0.100
	R^2	0.976	0.979	0.978
Redlich–Peterson	K_{R-P} (L g^{-1})	5.131	5.385	4.709
	a_{R-P} (L mg^{-1})$^{\beta R-P}$	0.016	0.033	0.065
	β_{R-P}	0.857	0.900	0.950
	R^2	0.979	0.977	0.978
Khan	Q_m (mg g^{-1})	169.633	201.836	758.932
	b_K	0.030	0.026	0.006
	a_K	0.389	0.900	0.007
	R^2	0.979	0.979	0.978

For the three dyes, the R_L value was between 0 and 1, indicating that Langmuir isotherm was favorable. From this research work, the maximum monolayer coverage capacity (q_m) from Langmuir isotherm model was 833.333, 833.333 and 243.902 mg g^{-1}; Langmuir isotherm constants (K_l) were 0.006, 0.006 and 0.021 L mg^{-1}. The separation factor (R_L) was 0.770, 0.777 and 0.485, indicating that the equilibrium sorption was favorable and that R^2 values were 0.999, 0.991 and 0.984. These results prove that the sorption data fitted well with Langmuir isotherm model for MB, MG and MV, respectively.

A comparison study of the sorption capacity q_m (mg g^{-1}) of few adsorbents available in literature for the removal of MB, MG and MV from aqueous solutions are regrouped in Table 4.

It was clear that *A. graveolens* biosorbent used in the present work had a relatively high sorption capacity compared with other sorbents.

Table 4
Comparison of maximum adsorption capacities of *A. graveolens* with other adsorbents for MV in aqueous solutions

Adsorbents	Dyes	Q_m (mg g^{-1})	Ref.
Activated carbon	MV	500	[65]
N-benzyltriazole derivatized dextran	MV	95.24	[66]
Sunflower seed hulls	MV	92.59	[67]
Halloysite nanotubes	MV	105.26	[68]
Pu-erh tea powder	MV	277.78	[69]
Halloysite nanotube–Fe_3O_4	MV	90.09	[70]
Ammodaucus leucotrichus	MV	500	[71]
A. graveolens	MV	243.90	Present work
Montmorillonite	MG	40.48	[72]
Sargassum swartzii	MG	76.92	[4]
Rubber wood sawdust	MG	25.8–36.3	[73]
Bentonite clay	MG	7.72	[74]
Pleurotus ostreatus	MG	32.33	[75]
Tamarind fruit shell	MG	1.95	[76]
Turbinaria conoides	MG	66.6	[77]
A. graveolens	MG	833.33	Present work
Cedar sawdust	MB	111.96	[78]
Crushed brick	MB	80.60	[78]
Beech sawdust	MB	13.6	[79]
Spinel magnesium aluminate nanoparticles	MB	0.945	[80]
Elaeagnus angustifolia	MB	227.27	[81]
Citrus limetta	MB	227.3	[82]
Banana leaves	MB	109.9	[83]
A. graveolens	MB	833.33	Present work

So, *A. graveolens* is a suitable biomass for the removal of MB, MG and MV from aqueous solutions with q_m equal to 833.33, 833.33 and 243.9 mg g^{-1}, respectively.

The n value, a constant indicating the adsorption intensity or surface heterogeneity, was 1.079, 1.117 and 1.079 for MB, MG and MV, respectively, which indicated a favorable sorption process since $1 < n < 10$ [84]. Approximate indicators of sorption capacity, constant K_F, were 5.466, 5.537 and 5.156 L mg^{-1} for MB, MG and MV, respectively, while R^2 values are >0.98.

Temkin equation demonstrated that the values of K_t were equal to 0.382, 0.491 and 0.409 L g^{-1}, and those of B_1 were equal to 38.482, 29.090 and 34.675 J mol^{-1} for MB, MG and MV, respectively; these results clearly indicated a physical sorption process. The values of R^2 were equal to 0.978, 0.997 and 0.925. For Dubinin–Radushkevich model, q_m was equal to 67.952, 56.328 and 57.208 mg g^{-1} for MB, MG and MV, respectively. The mean free energy was equal to 0.382, 0.491 and 0.409 kJ mol^{-1}, indicating a physisorption process; the values of R^2 were equal to 0.906, 0.956 and 0.811 for MB, MG and MV, respectively.

Generally, R^2 values of the Sips isotherm model for all dyes tested were higher than the other fitted models, showing that the equilibrium experimental data were better explained by the Sips equation where the value of this constant is higher than 0.993. This statement was revealed by many authors, since that Sips isotherm is a combination of the Langmuir and Freundlich isotherm models. Also, all maximum sorption capacities of Sips model are lower than Langmuir model.

For the Khan and Toth models, R^2 and maximum sorption capacity values for all dyes tested were lower than Langmuir model, but with MV, the maximum sorption capacity of Khan model is higher. This is owing to the fact that this model is derived from potential theory and is applicable to heterogeneous sorptions, which generally indicate that the adsorption sites are energetically homogeneous. Also, most sites have sorption energy less than the mean value [11].

Comparison of values of exponent $B_{R–P}$ (obtained from R–P model) has also triggered interesting results. The values of $B_{R–P}$ are lower than 1; they were found in the range from 0,857 to 0.980. This result is attributed to the presence of a solid impediment between the pores and the large molecules of the adsorbate (dye). Moreover, the value of the exponent $B_{R–P}$ (from the R–P isotherm) affected the shape of the isotherm; according to Wu et al. [85,86], the higher the g value (up to 1) the more significant the curvature of the isotherm (i.e., the sharper the increase of the adsorbed amount at the beginning with more horizontal end of the curve).

4. Conclusion

The present study indicated that *A. graveolens* biomass exhibited high sorption performance for the removal of dyes. The sorption efficiency was determined as a function of the initial adsorbate concentration, pH, adsorbent dosage and agitation speed. SEM-EDX analysis shows the homogeneity of the surface and composition of biomass. FTIR characterization of *A. graveolens* suggested that the surface chemistry of the biomass played an important role in understanding the sorption phenomenon. The optimal condition for the best biosorption of dyes were 300 rpm, optimal biomass concentration and at pH 4.02, 5.78 and 7.12 for MB, MG and MV, respectively. The pseudo-second-order kinetic equation could best describe the efficient removal of dyes by *A. graveolens*. The intraparticle diffusion model indicated that the process is partially controlled by the boundary layer and Bangham's equation shows that the film diffusion was not the only rate-controlling parameter.

The isotherms study showed that the maximum monolayer sorption capacities were found using Langmuir isotherm model as 833.333, 833.333 and 243.902 mg g^{-1} for MB, MG and MV, respectively. Sips and Freundlich isotherm models best fitted onto the experimental data of MV removal while the Sips, Langmuir and Temkin isotherm models best fitted onto the experimental data of MG removal; however, for MB removal, Freundlich, Sips and Langmuir isotherm models were best fitted onto the experiment data.

References

[1] S. Srivastava, R. Sinha, D. Roy, Toxicological effects of malachite green, Aquat. Toxicol., 66 (2004) 319–329.
[2] Z. Aksu, Application of biosorption for the removal of organic pollutants: a review, Process Biochem., 40 (2005) 997–1026.
[3] M. Jerold, C. Vigneshwaranm, V. Sivasubramanian, Macrophytes: a potent bio-sorbent for the sequestration of heavy metals, Int. Adv. Res. J. Sci. Eng. Technol., 2 (2015) 16–26.

[4] M. Jerold, V. Sivasubramanian, Biosorption of malachite green from aqueous solution using brown marine macro algae *Sargassum swartzii*, Desal. Wat. Treat., 57 (2016) 25288–25300.
[5] S. Yu, M. Liu, M. Ma, M. Qi, Z.L.C. Gao, Impacts of membrane properties on reactive dye removal from dye/salt mixtures by asymmetric cellulose acetate and composite polyamide nanofiltration membranes, J. Membr. Sci., 350 (2010) 83–91.
[6] M. Jerold, V. Sivasubramanian, Fabrication of hybrid nanoscale zero-valent iron-*Sargassum Swartzii* biocomposite for the removal of crystal violet from aqueous solution, Int. J. Phytorem., 19 (2017) 214–224.
[7] E. Aladag, B.A. Fil, R. Boncukcuoglu, O. Sozudogru, A.E. Yılmaz, Adsorption of Methyl Violet dye a textile industry effluent onto montmorillonite – batch study, J. Dispersion Sci. Technol., 35 (2014) 1737–1744.
[8] B.A. Fil, C. Ozmetin, Adsorption of cationic dye from aqueous solution by clay as an adsorbent: thermodynamic and kinetic studies, J. Chem. Soc. Pak., 34 (2012) 896–906.
[9] B.A. Fil, Isotherm, kinetic, and thermodynamic studies on the adsorption behavior of malachite green dye onto montmorillonite clay, Part. Sci. Technol., 34 (2016) 118–126.
[10] Y. Guo, Y. Liu, Adsorption properties of methylene blue from aqueous solution onto thermal modified rectorite, J. Dispersion Sci. Technol., 35 (2013) 1351–1359.
[11] B.A. Fil, M. Korkmaz, C. Ozmetin, Application of nonlinear regression analysis for methyl violet (MV) dye adsorption from solutions onto illite clay, J. Dispersion Sci. Technol., 37 (2016) 991–1001.
[12] M. Korkmaz, C. Özmetin, B.A. Fil, E. Özmetin, Y. Yaşar, Methyl violet dye adsorption onto clinoptilolite (natural zeolite): isotherm and kinetic study, Fresenius Environ. Bull., 22 (2013) 1524–1533.
[13] K. Vijayaraghavan, Y.S. Yun, Bacterial biosorbents and biosorption, Biotechnol. Adv., 26 (2008) 266–291.
[14] L.A. Sepúlveda, F.A. Cuevas, E.G. Contreras, Valorization of agricultural wastes as dyes adsorbents: characterization and adsorption isotherms, Environ. Technol., 36 (2015) 913–923.
[15] Z. Aksu, S. Ertugrul, G. Dönmez, Methylene Blue biosorption by *Rhizopus arrhizus*: effect of SDS (sodium dodecylsulfate) surfactant on biosorption properties, Chem. Eng. J., 158 (2010) 474–481.
[16] R. Apiratikul, P. Pavasant, Sorption isotherm model for binary component sorption of copper, cadmium, and lead ions using dried green macroalga, *Caulerpa lentillifera*, Chem. Eng. J., 119 (2006) 135–145.
[17] D. Sud, G. Mahajan, M.P. Kaur, Agricultural waste material as potential adsorbent for sequestering heavy metal ions from aqueous solutions—a review, Bioresour. Technol., 99 (2008) 6017–6027.
[18] J. Wang, C. Chen, Biosorption of heavy metals by *Saccharomyces cerevisiae*: a review, Biotechnol. Adv., 24 (2006) 427–451.
[19] G. Crini, P.M. Badot, Application of chitosan, a natural aminopolysaccharide, for dye removal from aqueous solutions by adsorption processes using batch studies: a review of recent literature, Prog. Polym. Sci., 33 (2008) 399–447.
[20] S.J. You, J.Y. Teng, Anaerobic decolorization bacteria for the treatment of azo dye in a sequential anaerobic and aerobic membrane bioreactor, J. Taiwan Inst. Chem. Eng., 40 (2009) 500–504.
[21] P. Kaushik, A. Malik, Fungal dye decolourization: recent advances and future potential, Environ. Int., 35 (2009) 127–141.
[22] S. Ertugrul, N.O. San, G. Donmez, Treatment of dye (Remazol Blue) and heavy metals using yeast cells with the purpose of managing polluted textile wastewaters, Ecol. Eng., 35 (2009) 128–134.
[23] V.K. Gupta, A. Rastogi, A. Nayak, Biosorption of nickel onto treated alga (*Oedogonium Hatei*): application of isotherm and kinetic models, J. Colloid Interface Sci., 342 (2010) 533–539.
[24] A. Mittal, V.K. Gupta, A. Malviya, J. Mittal, Process development for the batch and bulk removal and recovery of a hazardous, water-soluble azo dye (Metanil Yellow) by adsorption over waste materials (bottom ash and de-oiled soya), J. Hazard. Mater., 151 (2008) 821–832.
[25] A. Ahmad, M. Rafatullah, O. Sulaiman, M.H. Ibrahim, R. Hashim, Scavenging behaviour of meranti sawdust in the removal of methylene blue from aqueous solution, J. Hazard. Mater., 170 (2009) 357–365.
[26] R.P. Han, D.D. Ding, Y.F. Xu, W.H. Zou, Y.F. Wang, Y.F. Li, L. Zou, Use of ricehusk for the adsorption of Congo red from aqueous solution in column mode, Bioresour. Technol., 99 (2008) 2938–2946.
[27] P.L. Homagai, K.N. Ghimire, K. Inoue, Adsorption behavior of heavy metals onto chemically modified sugarcane bagasse, Bioresour. Technol., 101 (2010) 2067–2069.
[28] S. Schiewer, M. Iqbal, The role of pectin in Cd binding by orange peel biosorbents: a comparison of peels, depectinated peels and pectic acid, J. Hazard. Mater., 177 (2010) 899–907.
[29] M.H. Baek, C.O. Ijagbemi, O. Se-Jin, D.S. Kim, Removal of malachite green from aqueous solution using degreased coffee bean, J. Hazard. Mater., 176 (2010) 820–828.
[30] G. Crini, Non-conventional low-cost adsorbents for dye removal: a review, Bioresour. Technol., 97 (2006) 1061–1085.
[31] B. Samey, A.R. Toosi, Kinetics study of malachite green fading in the presence of TX-100, DTAB and SDS, Bull. Korean Chem. Soc, 30 (2009) 2051–2056.
[32] D. Podstawczyk, A. Witek-Krowiak, K. Chojnacka, Z. Sadowski, Biosorption of malachite green by eggshells: mechanism identification and process optimization, Bioresour. Technol., 160 (2014) 161–165.
[33] P.S. Vankar, R. Sarswat, A.K. Dwivedi, R. Shanker Sahu, An assessment and characterization for biosorption efficiency of natural dye waste, J. Cleaner Prod., 60 (2013) 65–70.
[34] T. Pulliah, Medicinal Plants in India, Regency Publications, New Delhi, 2002.
[35] D.K. Mondal, B.K. Nandi, M.K. Purkait, Removal of mercury(II) from aqueous solution using bamboo leaf powder: equilibrium, thermodynamic and kinetic studies, J. Environ. Chem. Eng., 1 (2013) 891–898.
[36] E. Demirbas, N. Dizge, M.T. Sulak, M. Kobya, Adsorption kinetics and equilibrium of copper from aqueous solutions using hazelnut shell activated carbon, Chem. Eng. J., 148 (2009) 480–487.
[37] A.L. Cazetta, A.M.M. Vargas, E.M. Nogami, M.H. Kunita, M.R. Guilherme, A.C. Martins, T.L. Silva, J.C.G. Moraes, V.C. Almeida, NaOH-activated carbon of high surface area produced from coconut shell: kinetics and equilibrium studies from the methylene blue adsorption, Chem. Eng. J., 174 (2011) 117–125.
[38] B. Hameed, I. Tan, A. Ahmad, Adsorption isotherm, kinetic modeling and mechanism of 2,4,6-trichlorophenol on coconut husk-based activated carbon, Chem. Eng. J., 144 (2008) 235–244.
[39] S.M. Hasany, M.H. Chaudhary, Sorption potential of Hare river sand for the removal of antimony from acidic aqueous solution, Appl. Radiat. Isot., 47 (1996) 467–71.
[40] R.K. Singh, S. Kumar, S. Kumar, A. Kumar, Development of parthenium based activated carbon and its utilization for adsorptive removal of *p*-cresol from aqueous solution, J. Hazard. Mater., 155 (2008) 523–535.
[41] B.H. Stuart, Infrared Spectroscopy: Fundamentals and Applications, Wiley, Hoboken, NJ, USA, 2004, pp. 46–87.
[42] M.F. Ahmad, S. Haydar, A.A. Bhatti, A J. Bari, Application of artificial neural network for the prediction of biosorption capacity of immobilized *Bacillus Subtilis* for the removal of cadmium ions from aqueous solution, Biochem. Eng. J., 84 (2014) 83–90.
[43] G. Walker, L. Hansen, J. Hanna, S. Allen, Kinetics of a reactive dye adsorption onto dolomitic sorbents, Water Res., 37 (2003) 2081–2089.
[44] Y. Zhu, P. Kolar, Adsorptive removal of *p*-cresol using coconut shell-activated char, J. Environ. Chem. Eng., 2 (2014) 2050–2058.
[45] M. Dogan, Y. Ozdemir, M. Alkan, Adsorption kinetics and mechanism of cationic methyl violet and methylene blue dyes onto sepiolite, Dyes Pigm., 75 (2007) 701–713.
[46] S.A. Cárdenas, S.L. Cortez, M.C. Mazón, J.C.M. Gutiérrez, Study of malachite green adsorption by organically modified clay using a batch method, Appl. Surf. Sci., 280 (2013) 74–78.

[47] M. El Haddad, A. Regti, R. Slimani, S. Lazar, Assessment of the biosorption kinetic and thermodynamic for the removal of safranin dye from aqueous solutions using calcined mussel shells, J. Ind. Eng. Chem., 20 (2014) 717–724.
[48] I.D. Mall, V.C. Srivastava, G.V.A. Kumar, I.M. Mishra, Characterization and utilization of mesoporous fertilizer plant waste carbon for adsorptive removal of dyes from aqueous solution, Colloids Surf., A, 278 (2006) 175–187.
[49] M. Alkan, O. Demirbas, M. Dogan, Electrokinetic properties of sepiolite suspensions in different electrolyte media, J. Colloid Interface Sci., 281 (2005) 240–248.
[50] P. Ahuja, R. Gupta, R.K. Saxena, Zn^{2+} biosorption by *Oscillatoria anguistissima*, Process Biochem., 34 (1999) 77–85.
[51] M. Kilic, E.A. Varol, A.E. Pütün, Adsorptive removal of phenol from aqueous solutions on activated carbon prepared from tobacco residues: equilibrium, kinetics and thermodynamics, J. Hazard. Mater., 189 (2011) 397–403.
[52] Y. Zhu, P. Kolar, Adsorptive removal of p-cresol using coconut shell-activated char, J. Environ. Chem. Eng., 2 (2014) 2050–2058.
[53] I.D. Mall, V.C. Srivastava, N.K. Agarwal, Removal of Orange-G and Methyl Violet dyes by adsorption onto bagasse fly ash kinetic study and equilibrium isotherm analyses, Dyes Pigm., 69 (2006) 210–223.
[54] L. Das, P. Kolar, J.A. Osborne, J.J. Classen, Adsorption of *p*-cresol on granular activated carbon, Agric. Eng. Int., 14 (2012) 37–49.
[55] Y.A. Yahaya, M.M. Don, S. Bhatia, Biosorption of copper(II) onto immobilized cells of *Pycnoporus sanguineus* from aqueous solution: equilibrium and kinetic studies, J. Hazard. Mater., 161 (2009) 189–195.
[56] E. Bagda, N.A. Zonuz, Uranyl ions removal by *Quercus macrenthera* gall's extract-based cryogels with extreme characteristics, Clean, 42 (2014) 1816–1823.
[57] Y.S. Ho, G. McKay, Pseudo-second order model for sorption processes, Process Biochem., 34 (1999) 451–465.
[58] N. Kannan, M. Sundaram, Kinetics and mechanism of removal of methylene blue by adsorption on various carbons a comparative study, Dyes Pigm., 51 (2001) 25–40.
[59] Q. Sun, L. Yang, The adsorption of basic dyes from aqueous solution on modified peat- resin particle, Water Res., 37 (2003) 1535–1544.
[60] F. Akbal, Sorption of phenol and 4-chlorophenol onto pumice treated with cationic surfactant, J. Environ. Manage., 74 (2005) 239–244.
[61] A.M. Din, B. Hameed, A. Ahmad, Batch adsorption of phenol onto physiochemical-activated coconut shell, J. Hazard. Mater., 161 (2009) 1522–1529.
[62] M. Dogan, Y. Ozdemir, M. Alkan, Adsorption kinetics and mechanism of cationic methyl violet and methylene blue dyes onto sepiolite, Dyes Pigm., 75 (2007) 701–713.
[63] Y.S. Ho, G. McKay, Sorption of dye from aqueous solution by peat, Chem. Eng. J., 70 (1998) 115–124.
[64] M. Dogan, M. Alkan, A. Türkyilmaz, Y. Özdemir, Kinetics and mechanism of removal of methylene blue by adsorption onto perlite, J. Hazard. Mater., 109 (2004) 141–148.
[65] S. Chen, J. Zhang, C. Zhang, Q. Yue, Y. Li, C. Li, Equilibrium and kinetic studies of methyl orange and methyl violet adsorption on activated carbon derived from *Phragmites australis*, Desalination, 252 (2010) 149–156.
[66] E. Cho, M.N. Tahir, H. Kim, J.H. Yu, S. Jung, Removal of methyl violet dye by adsorption onto *N*-benzyltriazole derivatized dextran, RSC Adv., 43 (2015) 327–334.
[67] B.H. Hameed, Equilibrium and kinetic studies of methyl violet sorption by agricultural waste, J. Hazard. Mater., 154 (2008) 204–212.
[68] R. Liu, B. Zhang, D. Mei, H. Zhang, J. Liu, Adsorption of methyl violet from aqueous solution by halloysite nanotubes, Desalination, 268 (2011) 111–116.
[69] P. Li, Y.J. Su, Y. Wang, B. Liu, L.M. Sun, Bioadsorption of methyl violet from aqueous solution onto Pu-erh tea powder, J. Hazard. Mater., 179 (2010) 43–48.
[70] J. Duan, R. Liu, T. Chen, B. Zhang, J. Liu, Halloysite nanotube-Fe_3O_4 composite for removal of methyl violet from aqueous solutions,Desalination,293 (2012) 46–52.
[71] A. Hamitouche, S. Benammar, M. Haffas, A. Boudjemaa, K. Bachari, Biosorption of methyl violet from aqueous solution using Algerian biomass, Desal. Wat. Treat., 57 (2016) 15862–15872.
[72] S.A. Cárdenas, S.L. Cortez, M.C. Mazón, J.C.M. Gutiérrez, Study of malachite green adsorption by organically modified clay using a batch method, Appl. Surf. Sci., 280 (2013) 74–78.
[73] K.V. Kumar, S. Sivanesan, Isotherms for malachite green onto rubber wood (*Hevea brasiliensis*) sawdust: comparison of linear and non-linear methods, Dyes Pigm., 72 (2007) 124–129.
[74] S.S. Tahir, N. Rauf, Removal of a cationic dye from aqueous solutions by adsorption onto bentonite clay, Chemosphere, 63 (2006) 1842–1848.
[75] Z. Chen, H. Deng, C. Chen, Y. Yang, X. Heng, Biosorption of malachite green from aqueous solutions by *Pleurotus ostreatus* using Taguchi method, J. Environ. Health Sci. Eng., 12 (2014) 1–10.
[76] P. Saha, S. Chowdhury, S. Gupta, I. Kumar, R. Kumar, Assessment on the removal of malachite green using tamarind fruit shell as biosorbent, Clean, 38 (2010) 437–445.
[77] R. Rajesh Kannan, M. Rajasimman, N. Rajamohan, B. Sivaprakash, Brown marine algae *Turbinaria conoides* as biosorbent for malachite green removal: equilibrium and kinetic modeling, Front. Environ. Sci. Eng. China, 4 (2010) 116–122.
[78] O. Hamdaoui, Batch study of liquid-phase adsorption of methylene blue using cedar sawdust and crushed brick, J. Hazard. Mater., 135 (2006) 264–273.
[79] F.A. Batzias, D.K. Sidiras, Simulation of methylene blue adsorption by salts-treated beech sawdust in batch and fixed-bed systems, J. Hazard. Mater., 149 (2007) 8–17.
[80] B. Ismail, S.T. Hussain, S. Akram, Adsorption of methylene blue onto spinel magnesium aluminate nanoparticles: adsorption isotherms, kinetic and thermodynamic studies, Chem. Eng. J., 219 (2013) 395–402.
[81] M. Rahimdokht, E. Pajootan, M. Arami, Central composite methodology for methylene blue removal by *Elaeagnus angustifolia* as a novel biosorbent, J. Environ. Chem. Eng., 4 (2016) 1407–1416.
[82] S. Shakoor, A. Nasar, Removal of methylene blue dye from artificially contaminated water using *Citrus limetta* peel waste as a very low cost adsorbent, J. Taiwan Inst. Chem. Eng., 66 (2016) 154–163.
[83] R.R. Krishni, K.Y. Foo, B.H. Hameed, Adsorptive removal of methylene blue using the natural adsorbent-banana leaves, Desal. Wat. Treat., 52 (2014) 6104–6112.
[84] N. Abidi, J. Duplay, F. Ayari, S. Gangloff, M. Trabelsi-Ayadi, Adsorption of anionic dye on natural and organophilic clays: effect of textile dyeing additives, Desal. Wat. Treat., 54 (2015) 1754–1769.
[85] F.C. Wu, B.L. Liu, K.-T. Wu, R.-L. Tseng, A new linear form analysis of Redlich-Peterson isotherm equation for the adsorptions of dyes, Chem. Eng. J., 162 (2010) 21–27.
[86] L. Bartonova, L. Ruppenthalova, M. Ritz, Adsorption of Naphthol Green B on unburned carbon: 2- and 3- parameter linear and non-linear equilibrium modelling, Chin. J. Chem. Eng., 25 (2017) 37–44.